ELSEVIER

Solid State Ionics 109 (1998) 285–294

SOLID STATE IONICS

Synthesis of spinel $LiMn_2O_4$ cathode material prepared by an adipic acid-assisted sol–gel method for lithium secondary batteries

Yun-sung Lee[a], Yang-Kook Sun[b,*], Kee-Suk Nahm[a]

[a]*Department of Chemical Technology, College of Engineering, Chonbuk National University, Chonju 561-756, South Korea*
[b]*Polymer Materials Laboratory, Chemical Sector, Samsung Advanced Institute of Technology, 103-12, Moonji-Dong, Yusong-Gu, Daejon 305-380, South Korea*

Received 24 October 1997; accepted 4 February 1998

Abstract

The spinel $LiMn_2O_4$ powders were synthesized at 300–800°C for 10 h in air by a sol–gel method using adipic acid as a chelating agent. The dependence of the physicochemical properties of the spinel $LiMn_2O_4$ powders such as crystallinity, lattice constant *a*, and specific surface area on calcination temperature and adipic acid quantity was extensively investigated. The physicochemical properties of the $LiMn_2O_4$ powders could be controlled by simply varying the processing condition of pyrolysis and the quantity of chelating agent. The charge–discharge characteristics and the cycling behavior of Li/1 M $LiBF_4$–EC/DEC electrolyte/$LiMn_2O_4$ cells revealed that $LiMn_2O_4$ electrode calcined at higher temperatures showed a high initial capacity, while the electrode calcined at lower temperatures exhibited a good cycling behavior.

Keywords: Lithium secondary batteries; Lithium manganese oxides; Sol–gel method; Chelating agent; Adipic acid

1. Introduction

The layered oxides, $LiMO_2$ (M = Co, Ni and Mn) and spinel $LiMn_2O_4$ are the most widely studied 4 V cathode materials for lithium secondary batteries with high energy density [1–8]. Among these, the spinel $LiMn_2O_4$ has been investigated extensively as the most promising cathode material for lithium secondary batteries because of its low cost, easy preparation and environmental advantages [5–8].

$LiMn_2O_4$ powders are usually prepared by a solid-state reaction of lithium salt such as lithium hydroxide, carbonate, or nitrate and manganese oxide, hydroxide, or carbonate powders at either low (400 to 600°C) or high temperatures (700 to 800°C) [5–10]. However, this method has several disadvantages; inhomogeneity, irregular morphology, larger particle size with broader particle size distribution, poor control of stoichiometry, and longer periods of calcination followed by extended grinding. In order to achieve the efficient Li utilization at high rates of charge–discharge and the reliability of lithium secondary batteries, it is necessary to obtain submicron sized particles with a uniform morphology, narrow size distribution, and homogeneity.

It was reported that the quantity of $LiMn_2O_4$ powders used for lithium secondary batteries was

*Corresponding author. Tel.: +82-42-865-4074; fax: +82-42-865-4075; e-mail: yksun@saitgw.sait.samsung.co.kr

0167-2738/98/$19.00
PII: S0167-2738(98)00085-X

strongly dependent on the synthetic method of the materials [11]. Considerable improvements have been made in the preparation of high-performance cathode active materials by using a solution method for lithium secondary batteries [10–14]. Among the solution methods, a sol–gel method can produce highly homogeneous powders of increased surface area, which enhance the performance of the electrode. This simple method has some advantages such as good stoichiometric control and production of submicron-sized particles with narrow particle-size distribution, relatively shorter processing time, and lower calcination temperature. In spite of these advantages, there have been a few reports on the preparation of $LiMn_2O_4$ powders by a sol–gel method [12–15]. Recently, the author has reported that ultrafine $LiCoO_2$ powders, highly homogeneous $LiCoO_2$ powders, crystalline $LiNiO_2$ powders, and phase-pure $Li_{1.03}Mn_2O_4$ powders could be successfully synthesized using the sol–gel method [16–19]. It is well known that the physicochemical properties of oxide powders strongly depend on the chelating agent used in the sol–gel method [20]. In practice, it is important to determine an optimum condition under which $LiMn_2O_4$ powders with desired electrochemical properties can be synthesized.

In this study, $LiMn_2O_4$ powders were synthesized by a sol–gel method using adipic acid as a chelating agent. The main interest of this work is to investigate the effects of the molar ratio of adipic acid to total metal ions and the calcination temperature on the physicochemical properties and charge–discharge behavior of $LiMn_2O_4$ powders synthesized.

2. Experimental

$LiMn_2O_4$ powders were prepared along a synthetic procedure as shown in Fig. 1. A stoichiometric amount of Li (Kanto Chemical Co., Reagent grade) and Mn acetate (Acros Co., high purity) salts with the cationic ratio of Li:Mn = 1:2 were dissolved in the distilled water and mixed well with an aqueous solution of adipic acid (Shimakyu's purechemical Co., EP grade). The solution was evaporated at 90°C for 12 h to form a transparent sol. The resultant sol was dried at 90–100°C for 24 h in a vacuum dryer to yield gel precursors. For the preparation of the gel

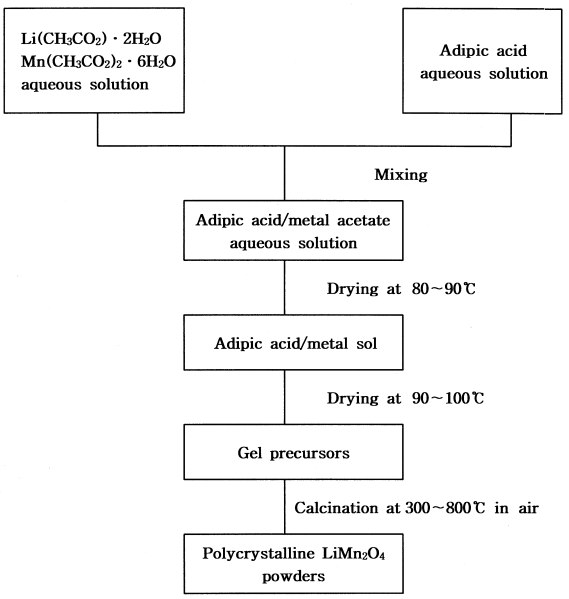

Fig. 1. Synthetic procedure of polycrystalline $LiMn_2O_4$ powders by the adipic acid-assisted sol–gel method.

precursors with different molar ratio of adipic acid to total metal ions, the same procedure was repeated at various molar ratio of 0.5, 0.83, 1.5 and 2.0. The gel precursors were decomposed at 300°C for 10 h in air to eliminate organic contents. The decomposed powders were slightly ground and then calcined at 300–800°C for 10 h in air to obtain phase-pure polycrystalline $LiMn_2O_4$ powders.

The thermal decomposition behavior of the gel precursors was examined by means of thermogravimetric analyzer (TGA, DuPont, TA2000). Powder X-ray diffraction (XRD, D/Max-3A, Rigaku) using Cu Kα radiation was used to identify the crystalline phase of the materials calcined at various temperatures. Rietveld refinement was then performed with XRD data to obtain the lattice constant. The particle morphology of gel precursor materials before and after the calcination was observed using a scanning electron microscope (SEM, GEOL, JSM 6400). The specific surface area of the materials was measured by the BET method (Autosorb-1, Quantachrome) with nitrogen adsorption.

The electrochemical properties of $LiMn_2O_4$ powders were determined in a three-electrode electrochemical cell. The reference and counter electrodes

were constructed from the lithium foil (Cyprus Foote Mineral Co.). The electrolyte used was a 1:1 mixture of ethylene carbonate (EC) and diethyl carbonate (DEC) containing 1 M $LiBF_4$ (Mitsubishi Co.). The cathode was a mixture of 72 wt.% active material, 20 wt.% ketjenblack EC and 8 wt.% Teflon binder. The mixture was then dispersed in isopropyl alcohol and spread on Exmet, followed by pressing and drying at 120°C for 3 h. After the cells were assembled in a argon-filled dry box, the charge–discharge cycling was galvanostatically performed at a current density of 1 mA/cm^2 (a rate of 0.5 C) with cut-off voltage of 3.6 to 4.3 V (vs. Li/Li^+).

3. Results and discussion

The gel precursors were synthesized at various molar ratios of adipic acid to total metal ions. The milky color of the gel precursors indicated that the composition of the precursors was very homogeneous. It is believed that carboxylic groups in the adipic acid form a chemical bonding with the metal ions so that they become extremely viscous gelled polymeric resins [15,19,21,22].

The weight loss of the gel precursors was measured with temperature using TGA and compared to those of sole adipic acid and the mixture of metal acetate (Li:Mn acetate = 1:2) in Fig. 2. The figure shows that the weight loss of the adipic acid

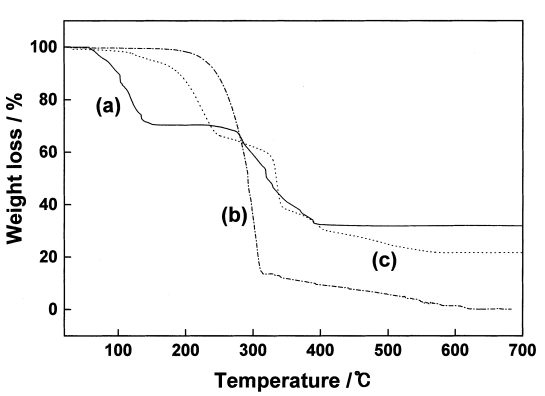

Fig. 2. Thermogravimetric analysis for (a) the mixture of metal acetate (Li:Mn acetate = 1:2), (b) sole adipic acid, and (c) the gel precursors pretreated in a vacuum dryer at 100°C prior to thermal analysis in air at the heating rate of 5°C/min.

decreases abruptly at around 270°C, slowly until the temperature increases up to 620°C, and levels off. For the mixture of metal acetate, however, two discrete weight losses are observed at the temperature ranges of 23–138°C and 275–390°C. The first loss is originated from the removal of water and the second one from the decomposition of acetate ions. In the case of the gel precursor, three discrete weight loss regions are detected at the temperature ranges of 140–275°C, 275–345°C and 345–600°C, and the weight loss of the precursor terminates at 575°C. The weight loss in the temperature range of 140–275°C corresponds to the removal of water, which is well consistent with the pyrolysis of the mixture of acetate. The weight loss in the temperature range of 275–345°C is associated with the decomposition of adipic acid and acetate ions. The adipic acid and the mixture of metal acetate are pyrolyzed at around 290°C and 290–390°C, respectively. The weight loss in the temperature range of 345–600°C is attributed to the combustion of the remaining organic constituents. It appears that adipic acid functions as a fuel in the decomposition of the acetate ions and heat evolved from the decomposition of acetate ions accelerates the decomposition of the remaining organic constituents. Similar behavior was observed in our previous work, which reported that a violent oxidation–decomposition reaction occurred at 320°C in the decomposition process of the gel precursors. We prepared the gel precursors by the sol–gel method using glycolic acid as a chelating agent [19].

In order to investigate the effect of the quantity of chelating agent on the formation mechanism and structural difference of the spinel $LiMn_2O_4$ phase, the precursor materials calcined at 300 and 800°C were analyzed with XRD.

Fig. 3 shows XRD patterns for the gel-derived materials calcined at 300°C for 10 h in air in terms of the molar ratio of adipic acid to total metal ions. For the materials prepared at the molar ratio of 0.5 and 0.83, the peaks of impurities such as β-MnO_2, Mn_2O_3 and Li_2CO_3 are observed with $LiMn_2O_4$ spinel phase. But, a closer observation of the figure reveals that the ratio of the amount of the $LiMn_2O_4$ spinel phase to that of the impurity phases increases with the increase of adipic acid quantity, resulting in the improvement of $LiMn_2O_4$ quality. Meanwhile, the gel precursors synthesized at the molar ratio of

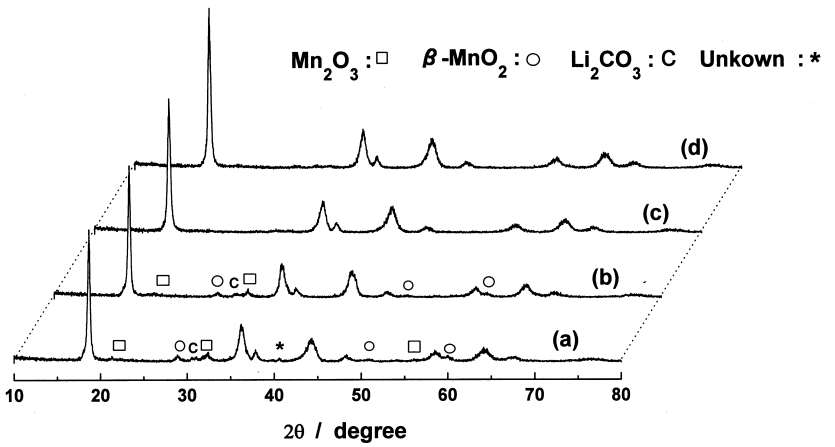

Fig. 3. X-ray diffraction patterns of $LiMn_2O_4$ powders prepared at various molar ratios of adipic acid to total metal ions of (a) 0.5, (b) 0.83, (c) 1.5, (d) 2.0. The gel precursors were calcined at 300°C for 10 h.

1.5 and 2.0 are crystallized into phase-pure $LiMn_2O_4$ spinel powders without any development of minor phase.

Fig. 4 shows the X-ray diffraction patterns for the materials calcined at 800°C for 10 h in air in terms of the quantity of adipic acid. It is confirmed from the XRD patterns that the spinel $LiMn_2O_4$ phase, which indexes to a cubic unit cell with a space group Fd3m, is formed regardless of the molar ratio of adipic acid to total metal ions. However, the comparison of peak intensities at each 2θ shows that the crystallinity of the materials is improved with increasing molar ratio of adipic acid to total metal ions.

Fig. 5 shows the effect of the quantity of chelating agent on the lattice constant of the cubic unit cell of the material prepared at the condition of Fig. 4. With the increase of the molar ratio from 0.5 to 2.0, the lattice constant increases linearly from

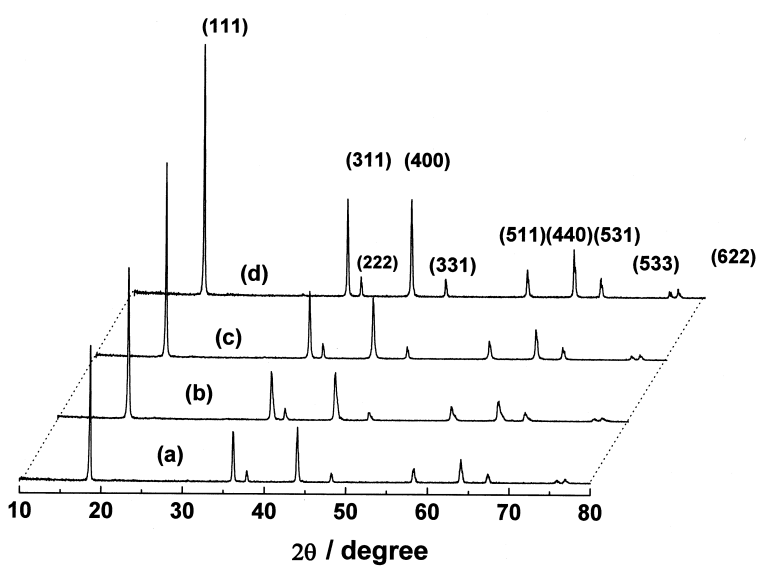

Fig. 4. X-ray diffraction patterns of $LiMn_2O_4$ powders prepared at various molar ratios of adipic acid to total metal ions of (a) 0.5, (b) 0.83, (c) 1.5, (d) 2.0. The gel precursors were calcined at 800°C for 10 h.

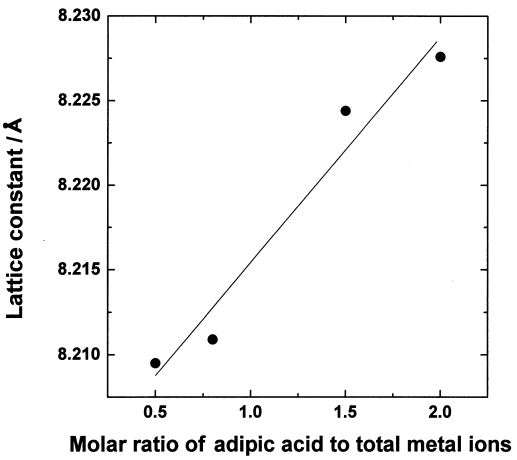

Fig. 5. Dependence of the lattice constant of $LiMn_2O_4$ powders calcined at 800°C on the molar ratio of adipic acid to total metal ions.

8.2095 to 8.2276 Å, which indicates the improvements of the crystallinity of the spinel $LiMn_2O_4$ powders.

The reason why the crystallinity and the specific surface area of the $LiMn_2O_4$ powders increase with the quantity of adipic acid used in the preparation of the gel precursors can be explained as follows; it is well known that the adipic acid not only functions as a chelating agent but also provides the heat of combustion required for the synthesis of $LiMn_2O_4$ powders [16–19,21]. XRD patterns in Figs. 3 and 4 showed that both spinel $LiMn_2O_4$ and impurity phases appeared from the gel precursors prepared at small quantity of adipic acid, while the gel precursors at large quantity of adipic acid were composed only of the pure-phase $LiMn_2O_4$ spinel powders. The smaller the amount of adipic acid used in the preparation of gel precursors, the shorter the Li–Mn cation distance, and thus the higher the probability of the crystallization between the cations, but lower homogeneity is observed in the gel precursors and less combustion heat is generated from adipic acid. On the contrary, at large amounts of adipic acid, the homogeneity of the gel precursors is better, more cross-linked gel precursors suppress cation mobility, and a large amount of the combustion heat is generated from the adipic acid. This causes the formation of the $LiMn_2O_4$ phase together with fluffy powders which result from much void volumes formed by the evolution of CO and CO_2 gases during the thermal decomposition of adipic acid. This is supported by the observation that the materials swell much when the amount of adipic acid increases though the gel precursors are calcinated at the same temperature. Therefore, it is considered that the increased amount of combustion heat might increase the crystallinity and the specific surface area of $LiMn_2O_4$ powders at large quantities of adipic acid.

Fig. 6 shows X-ray diffraction (XRD) patterns for the gel-derived materials calcined at various temperatures for 10 h in air. The molar ratio of adipic acid to total metal ions was 1.5. For the material calcined at 300°C, the crystallinity of $LiMn_2O_4$ spinel phase is poor, but the peaks of impurities such as Li_2CO_3, MnO_2 and Mn_2O_3 are not observed, which are often found in other low temperature techniques. It is interesting to note that the (220) diffraction line, which is originated only from the tetrahedral site (Li ion site) in the spinel structure, is not observed in the materials. This means that manganese ions are not displaced into tetrahedral sites and only lithium ions with very small scattering factor occupy the sites [23]. The higher the calcination temperature is, the sharper the intensities of diffraction peaks, and the better the crystallinity of the $LiMn_2O_4$ spinel phase. The precursors are crystallized into phase-pure $LiMn_2O_4$ spinel powders without any development of minor phase in the calcination temperature ranges. These results strongly suggest that this synthetic method is much su-

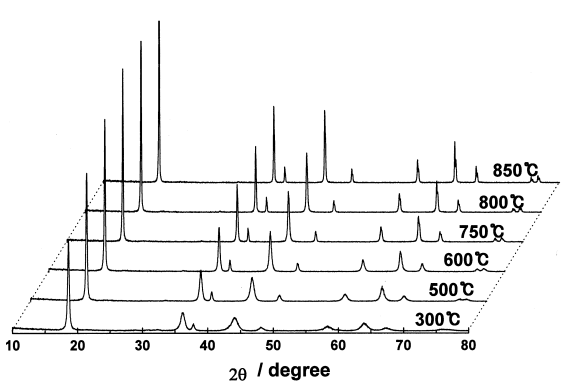

Fig. 6. X-ray diffraction patterns of gel derived materials calcined at various temperatures. The molar ratio of adipic acid to total metal ions was 1.5.

perior to the solid-state reaction since phase-pure $LiMn_2O_4$ spinel powders are prepared at much lower calcination temperature in a shorter calcination time. Similar results have already been observed in our previous reports on the preparations of $LiCoO_2$, $LiNiO_2$ and $Li_{1.03}Mn_2O_4$ powders by the sol–gel method using PAA, maleic acid, and glycolic acid as chelating agents [16–19].

Fig. 7 shows the effects of calcination temperature on the lattice constant of the cubic unit cell and crystallite size of the materials prepared at the condition of Fig. 6. The lattice constants were calculated by the Rietveld refinement on the XRD data. It is seen from Fig. 7 that the lattice constant increases almost linearly from 8.2058 to 8.2295 Å with increasing the calcination temperature from 300 to 850°C. It is reported that the value of the average oxidation state of manganese in the spinel phase is closely related to the lattice constant of the cubic unit cell [23–25]. Lower calcination temperatures result in the formation of a more oxidized manganese cation because manganese ions are stable preferentially as Mn^{4+} at lower temperatures [26]. The atomic radius of Mn^{4+} is smaller than that of Mn^{3+} and thus the lattice constant of the cubic unit cell of the materials calcined at higher temperatures is larger than that at lower temperatures. It is reported that the higher the oxidation state of manganese, the smaller the lattice parameter, and the broader the diffraction peaks of the materials calcined at lower temperature [24,25].

The crystallite size of the materials was calculated from full width at the half maximum (FWHM) of the (400) peak at $2\theta = 44°$. The crystallite size increases linearly from 70 to 300 nm as the calcination

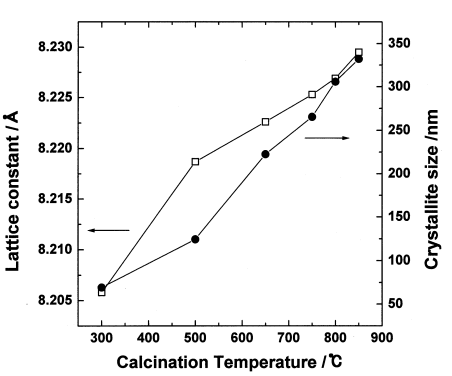

Fig. 7. Dependence of the lattice constant and crystallite size of $LiMn_2O_4$ powders on the calcination temperature when the molar ratio of adipic acid to total metal ions was 1.5.

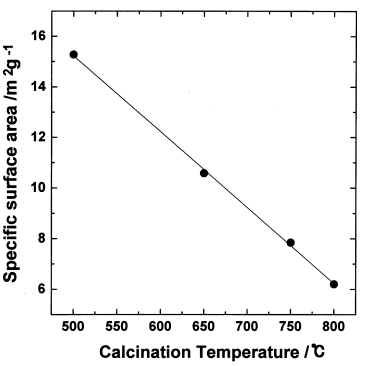

Fig. 8. Dependence of the specific surface area for $LiMn_2O_4$ powders on the calcination temperature when the molar ratio of adipic acid to total metal ions was 1.5.

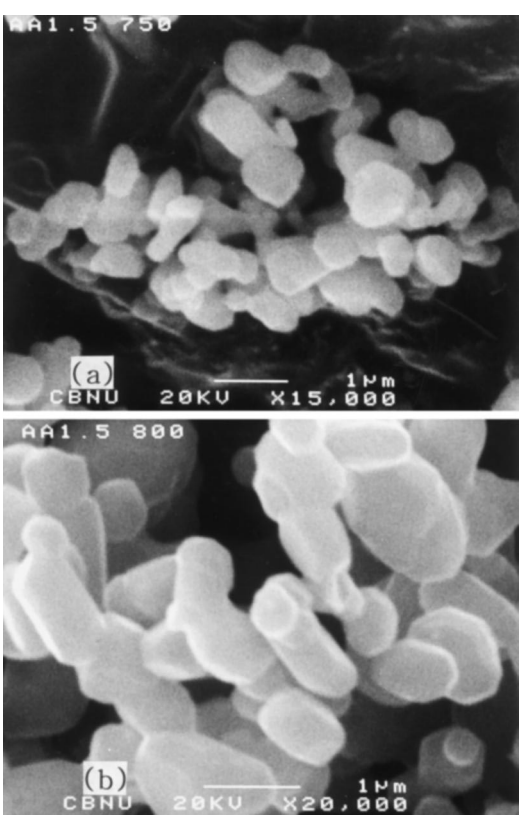

Fig. 9. Scanning electron micrographs of the $LiMn_2O_4$ powders calcined at (a) 750°C and (b) 800°C.

temperature increases from 300 to 800°C. It is well known that the crystallite size or the width of the Bragg peaks for the materials relates to the presence of the residual strain and is inversely proportional to the residual strain [12,23]. Lower crystallite size or higher residual strain may result from defects such as composition inhomogeneities, cationic mixing, grain boundaries, or polymorphism [12].

Fig. 8 shows the dependence of specific surface area on the calcination temperature. The specific surface area of the $LiMn_2O_4$ powders decreases linearly with increasing the calcination temperature. This is mainly due to the increase of particle size and the growth of $LiMn_2O_4$ crystallites as observed in the dependence of crystallite size on the temperature as shown in Fig. 7. The specific surface areas of the materials calcined at 500 and 800°C are 15.3 and 6.2 m^2/g, respectively. This ascribes to the fact that the

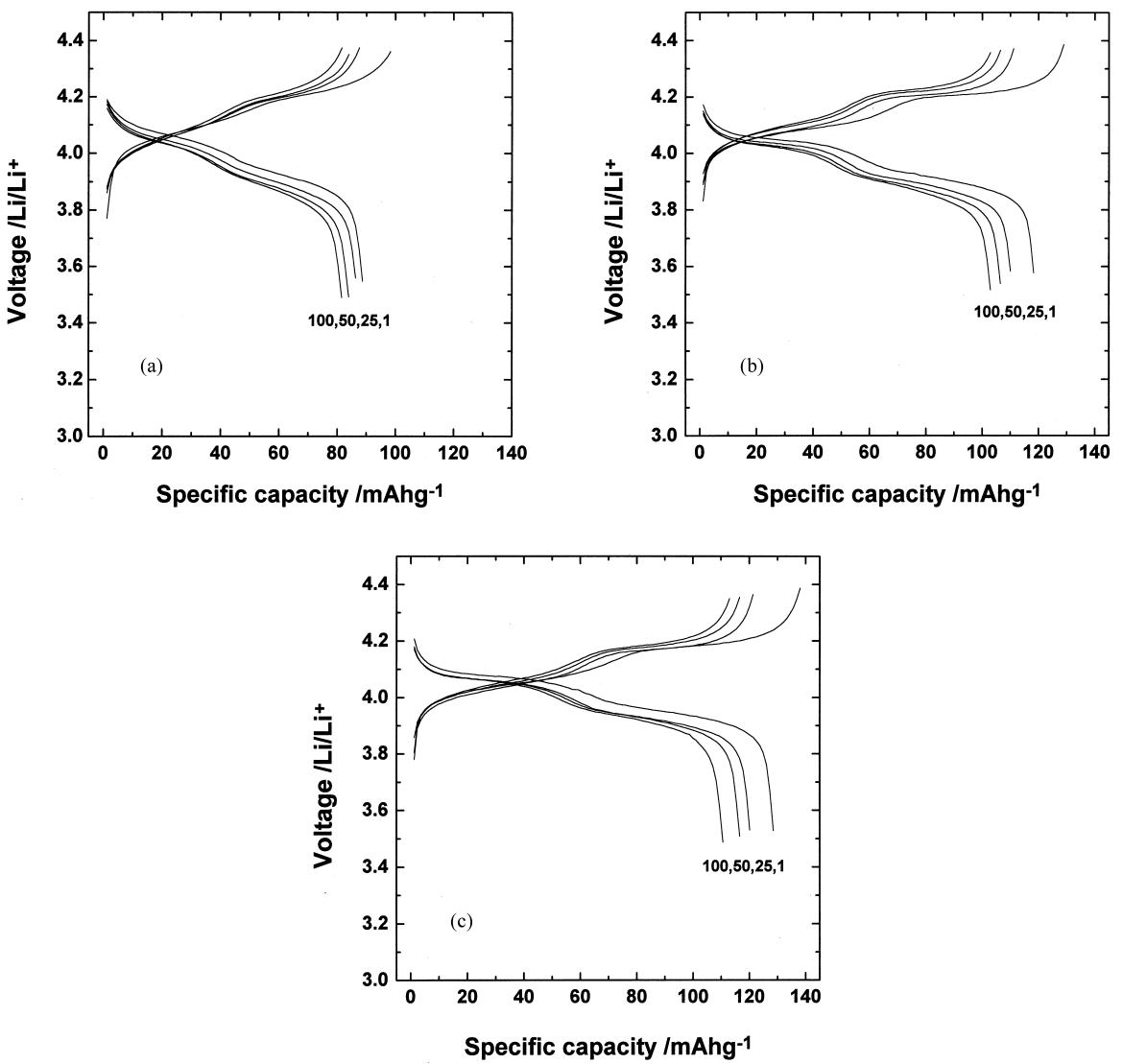

Fig. 10. Charge–discharge curves with the number of cycles for the Li/1 M $LiBF_4$–EC/DEC/$LiMn_2O_4$ cells using $LiMn_2O_4$ powders calcined at (a) 300, (b) 750 and (c) 800°C. Cycling was carried out galvanostatically at constant charge–discharge current density of 1 mA/cm^2 between 3.6 and 4.3 V.

materials derived from the gel precursors consist of small sized particles since they are of atomic scale and are homogeneously mixed with each other.

Fig. 9 shows SEM micrographs for the powders calcined at 750 and 800°C for 10 h in air. The gel precursors were prepared at the molar ratio of adipic acid to metal ions of 1.5. When the gel precursors are calcined at 750°C, the average particle size of the powders is 0.6 μm with a fairly narrow size distribution. Also, the shape of the powders is polygonal as seen in the solid-state reaction method. For the materials calcined at 800°C, it is observed that the particle size of the powders increases to about 1 μm with a narrow particle-size distribution.

Figs. 10 and 11 show the charge–discharge behavior and the discharge capacities of the Li/1 M $LiBF_4$–EC/DEC/$LiMn_2O_4$ cells with the cycle number at a constant charge–discharge current density of 1 mA/cm^2. $LiMn_2O_4$ powders were prepared at various calcination temperatures. The Li/1 M $LiBF_4$–EC/DEC/$LiMn_2O_4$ cells using $LiMn_2O_4$ powders calcined at higher temperatures such as 750 and 800°C (Fig. 10b and c) shows that the charge–discharge curves have two distinct plateaus near 4.0 and 4.16 V_{Li/Li^+}. It was known that each plateau delivers half of the total capacity. The appearance of the potential plateau near 4.0 V_{Li/Li^+} is due to the coexistence of two pseudophases of a lithium-diluted phase and a lithium-concentrated phase in a form of $Li_{0.5}Mn_2O_4$–$LiMn_2O_4$, but the plateau near 4.16 V_{Li/Li^+} is owing to the coexistence of λ-MnO_2–$Li_{0.5}Mn_2O_4$ [15]. On the contrary, the $LiMn_2O_4$ powders calcined at a lower temperature of 300°C (Fig. 10a) show that the charge–discharge curves have a slope in the potential range. No observation of potential plateau in this case indicates that lithium ion diffusion proceeds in a single phase of the low-crystalline electrode. The Li/1 M $LiBF_4$–EC/DEC/$LiMn_2O_4$ cells using $LiMn_2O_4$ powders calcined at 300, 750 and 800°C (Fig. 11) initially deliver 89, 118 and 128 mA h/g, respectively. The capacity slowly decreases with the cycle and remains 82, 103 and 113 mA h/g at the 100th cycles for the $LiMn_2O_4$ powders calcined at 300, 750 and 800°C, respectively. This shows very good capacity retention, especially in view of the relatively high charge–discharge current density of 1 mA/cm^2 or 0.5 C. The capacity retention over the 100th cycles are 88, 87 and 92% of the initial discharge capacity for the $LiMn_2O_4$ powders calcined at 300, 750 and 800°C, respectively. The poor crystallinity of $LiMn_2O_4$ powders calcined at lower temperatures is well consistent with the results of XRD patterns and the lattice constants as shown in Fig. 6 and Fig. 7, respectively. It is inferred from the above results that the $LiMn_2O_4$ powders calcined at higher temperatures have higher crystallinity and thus higher initial capacity, but fast capacity fading, due to Jahn–Teller distortion, is observed [27,28]. Similar behavior was reported in the previous works that the stability of the spinel host structure increases with decreasing the calcination temperature, which results in the creation of local defects, and the Jahn–Teller distortion has important effects on the capacity loss of $LiMn_2O_4$ [15,29].

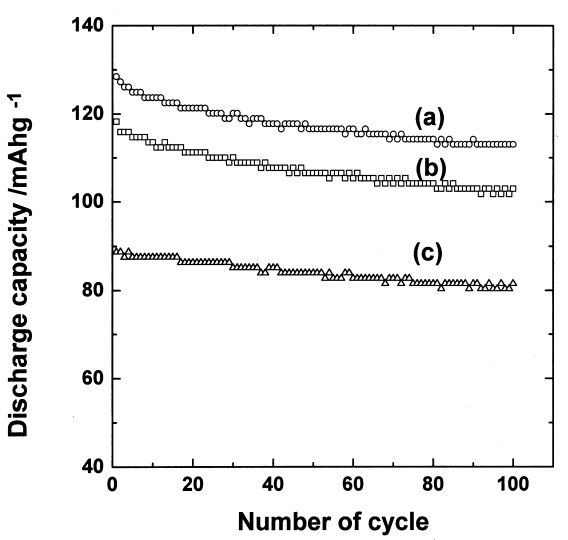

Fig. 11. Variation of specific discharge capacity with number of cycles for the Li/1 M $LiBF_4$–EC/DEC/$LiMn_2O_4$ cells using $LiMn_2O_4$ powders calcined at (a) 800, (b) 750 and (c) 300°C. Cycling was carried out galvanostatically at constant charge–discharge current density of 1 mA/cm^2 between 3.6 and 4.3 V.

To investigate the relation between the structure of the materials and the discharge capacity, the initial discharge capacity is plotted versus the lattice constant of the cubic unit cell and crystallite size of the powders in Fig. 12. The discharge capacity increases linearly with increasing both the lattice constant and crystallite size. The decreases of lattice constant and crystallite size of the materials (more Mn^{4+} than

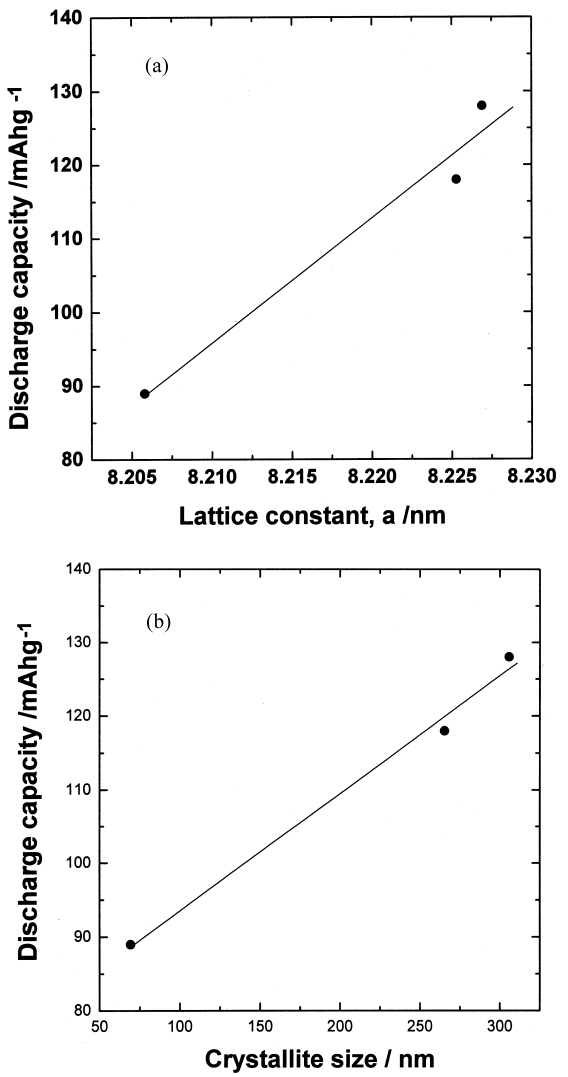

Fig. 12. Dependence of the discharge capacity on (a) lattice constant of cubic unit cell and (b) crystallite size of $LiMn_2O_4$ powders.

Mn^{3+}) calcined at lower temperature are due to imperfect spinel phase, which has a larger amount of cation vacancies and differences in the cation distribution between the tetrahedral and octahedral sites. Consequently, a low capacity is obtained in low crystalline material [24,25].

The adipic acid-assisted sol–gel method is a very attractive method for the synthesis of $LiMn_2O_4$-based cathode materials for lithium secondary batteries.

4. Conclusions

The spinel $LiMn_2O_4$ powders with submicron, narrow particle-size distribution, and excellent phase-pure particles were synthesized at 300–800°C for 10 h in air by a sol–gel method using an aqueous solution of metal acetate containing adipic acid as a chelating agent. The crystallinity of $LiMn_2O_4$ powders synthesized increased with increasing adipic acid quantity as well as calcination temperature. The specific surface area decreased with increase in the temperature. A wide variety of the physicochemical properties, such as crystallinity, particle size, and specific surface area of the powders, could be controlled by simply varying the processing condition of pyrolysis and the quantity of chelating agent. The $LiMn_2O_4$ powders with higher homogeneity in Li/1 M $LiBF_4$–EC/DEC electrolyte/$LiMn_2O_4$ cells had shown good discharge capacity and excellent cyclability. The high initial capacity and good cycling behavior of the $LiMn_2O_4$ powders were closely related to the higher crystallinity and retention of the spinel structure, respectively.

Acknowledgements

This study is supported by the academic research fund of the Ministry of Education, Republic of South Korea.

References

[1] K. Mizushima, P.C. Jones, P.J. Wiseman, J.B. Goodenouh, Mater. Res. Bull. 15 (1980) 783.
[2] C. Plichta, M. Salomon, S. Slane, M. Uchiyoma, B. Chua, W.B. Ebner, H.W. Lin, J. Power Sources 21 (1987) 25.
[3] J.R. Dahn, U. Von Sacken, C.A. Michel, Solid State Ionics 44 (1990) 87.
[4] R.J. Gummow, D.C. Liles, M.M. Thackeray, Mater. Res. Bull. 28 (1993) 1249.
[5] T. Ohuzuka, M. Kitagawa, T. Hirai, J. Electrochem. Soc. 137 (1990) 760.
[6] W.J. Macklin, R.J. Neat, R.J. Powell, J. Power Sources 34 (1991) 39.
[7] V. Manev, A. Momchilov, A. Nassalevska, A. Kozawa, J. Power Sources 41 (1993) 305.
[8] D. Guyomard, J.M. Tarascon, Solid State Ionics 69 (1994) 222.

[9] T. Nagaura, M. Yokokawa, T. Hasimoto, US Pat. 4,828,834.
[10] M.M. Thackeray, P.J. Johnson, L.A. De Picciotto, P.G. Bruce, J.B. Goodenough, Mater. Res. Bull. 19 (1984) 179.
[11] Y. Gao, J.R. Dahn, J. Electrochem. Soc. 143 (1996) 100.
[12] P. Barboux, J.M. Tarascon, F.K. Shokoohi, J. Solid State Chem. 94 (1991) 185.
[13] T. Tsumura, A. Shimizu, M. Inagaki, J. Mater. Chem. 3 (1993) 995.
[14] S.R.S. Prabaharan, M.S. Michael, T.P. Kumar, A. Mani, K. Athinarayanaswamy, R. Gangadharan, J. Mater. Chem. 5 (1995) 1035.
[15] W. Liu, G.C. Farrington, F. Chaput, B. Dunn, J. Electrochem. Soc. 143 (1996) 879.
[16] Y.-K. Sun, I.-H. Oh, S.-A. Hong, J. Mater. Sci. 31 (1996) 3617.
[17] I.-H. Oh, S.-A. Hong, Y.-K. Sun, J. Mater. Sci. 32 (1997) 3177.
[18] Y.-K. Sun, I.-H. Oh, J. Mater. Sci. Lett. 16(1) (1997) 30.
[19] Y.-K. Sun, Solid State Ionics 100 (1997) 115.
[20] Y. Teraoka, H. Kakebayashi, I. Moriguchi, S. Kagawa, Chem. Lett. (1991) 673.
[21] P.A. Lessing, Ceram. Bull. 68 (1989) 1002.
[22] M.S.G. Baythoun, F.R. Sale, J. Mater. Sci. 17 (1982) 2757.
[23] T. Tsumura, A. Shimizu, M. Inagaki, Solid State Ionics 90 (1996) 197.
[24] D.H. Jang, Y.J. Shin, S.M. Oh, J. Electrochem. Soc. 143 (1996) 2204.
[25] C. Tsang, A. Manthiram, Solid State Ionics 89 (1996) 305.
[26] C. Masquelier, M. Tabuchi, K. Ado, R. Kanno, Y. Kobayashi, Y. Maki, O. Nakamura, J.B. Goodenough, Solid State Chem. 123 (1996) 255.
[27] R.J. Gummow, A. de Kock, M.M. Thackeray, Solid State Ionics 69 (1994) 59.
[28] Z. Jiang, K.M. Abraham, J. Electrochem. Soc. 143 (1996) 1591.
[29] W. Liu, K. Kwal, G.C. Farrington, J. Electrochem. Soc. 143 (1996) 3590.